Title

Trafficking and gating of hyperpolarization-activated cyclic nucleotide-gated channels are regulated by interaction with tetratricopeptide repeat-containing Rab8b-interacting protein (TRIP8b) and cyclic AMP at distinct sites.

Journal

The Journal of biological chemistry, 286(23)

ISSN

0021-9258

Authors

Han, Ye
Noam, Yoav
Lewis, Alan S
et al.

Publication Date

2011-06-01

DOI

10.1074/jbc.m111.236125

THE JOURNAL OF BIOLOGICAL CHEMISTRY VOL. 286, NO. 23, pp. 20823–20834, June 10, 2011

Trafficking and Gating of Hyperpolarization-activated Cyclic Nucleotide-gated Channels Are Regulated by Interaction with Tetratricopeptide Repeat-containing Rab8b-interacting Protein (TRIP8b) and Cyclic AMP at Distinct Sites*[S]

Received for publication, March 1, 2011, and in revised form, April 12, 2011 Published, JBC Papers in Press, April 19, 2011, DOI 10.1074/jbc.M111.236125

Ye Han[‡1], Yoav Noam[§¶‖1], Alan S. Lewis[‡], Johnie J. Gallagher[‡], Wytse J. Wadman[‖], Tallie Z. Baram[§¶], and Dane M. Chetkovich[‡2]**

*From the [‡]Davee Department of Neurology and Clinical Neurosciences and the **Department of Physiology, Northwestern University Feinberg School of Medicine, Chicago, Illinois 60611, the Departments of [§]Anatomy and Neurobiology and [¶]Pediatrics, University of California, Irvine, Irvine, California 92697-4475, and the [‖]Swammerdam Institute for Life Sciences, Center for NeuroScience, University of Amsterdam, 1098 SM Amsterdam, The Netherlands*

Ion channel trafficking and gating are often influenced by interactions with auxiliary subunits. Tetratricopeptide repeat-containing Rab8b-interacting protein (TRIP8b) is an auxiliary subunit for neuronal hyperpolarization-activated cyclic nucleotide-gated (HCN) channels. TRIP8b interacts directly with two distinct sites of HCN channel pore-forming subunits to control channel trafficking and gating. Here we use mutagenesis combined with electrophysiological studies to define and distinguish the functional importance of the HCN/TRIP8b interaction sites. Interaction with the last three amino acids of the HCN1 C terminus governed the effect of TRIP8b on channel trafficking, whereas TRIP8b interaction with the HCN1 cyclic nucleotide binding domain (CNBD) affected trafficking and gating. Biochemical studies revealed that direct interaction between TRIP8b and the HCN1 CNBD was disrupted by cAMP and that TRIP8b binding to the CNBD required an arginine residue also necessary for cAMP binding. In accord, increasing cAMP levels in cells antagonized the up-regulation of HCN1 channels mediated by a TRIP8b construct binding the CNBD exclusively. These data illustrate the distinct roles of the two TRIP8b-HCN interaction domains and suggest that TRIP8b and cAMP may directly compete for binding the HCN CNBD to control HCN channel gating, kinetics, and trafficking.

HCN[3] channels are encoded by the HCN1–4 gene family and mediate hyperpolarization-activated cation current, I_h, which plays an important role in regulating electrical activity of neurons (for review, see Refs. 1–3). HCN channel gating and trafficking to specific subcellular domains contribute critically to the multiple physiological roles of the channels, and regulation of these processes is important for normal physiological functions as well as in disease (4). Each pore-forming HCN subunit is composed of an intracellular N terminus, six transmembrane domains, and a large intracellular C-terminal tail that includes a group of 6 helices (A′-F′, C-linker) that links the transmembrane domains to a cyclic nucleotide binding domain (CNBD). Direct binding of cyclic nucleotides to the CNBD of HCN subunits facilitates channel availability by opening of channels at more physiological (less hyperpolarized) potentials and by speeding kinetics of activation (5–7).

In addition to being regulated by cAMP, HCN channels interact with numerous proteins that can influence their function (for review, see Ref. 8). Recent studies have demonstrated that in the brain, native HCN channels co-purify with TRIP8b (also called peroxin 5-like protein, PEX5L) (9), and consistent with a role as an auxiliary HCN channel subunit, TRIP8b regulates HCN channel trafficking, voltage gating, and kinetics *in vitro* and *in vivo* (9–11). The TRIP8b C terminus is highly homologous to the peroxisomal import protein, peroxin 5 (PEX5), and is comprised of two sets of three tetratricopeptide repeat (TPR) domains separated by a linker, a C-terminal tail, and a region enriched in acidic amino acids N-terminal to the first TPR set that is conserved in both PEX5 and TRIP8b (10, 12). The N terminus of TRIP8b shares no sequence homology to PEX5 and is subject to extensive alternative splicing that leads to expression of multiple distinct TRIP8b isoforms. We previously showed that the TRIP8b TPR sets together interact with the HCN1 C-terminal tripeptide, whereas a region including the conserved acidic domain and the first two TPR domains is required for independent interaction with the HCN1 channel C-linker and CNBD (10). Alternatively spliced TRIP8b isoforms differentially affect surface expression and thereby control HCN channel current density, whereas all TRIP8b isoforms exhibit negative regulation on channel gating and kinetics (10, 11).

Whether the distinct interaction sites are responsible for distinct functional effects of TRIP8b on HCN channels is

* This work was supported, in whole or in part, by National Institutes of Health Grants NS05595 and NS059934 (to D. M. C.), NS064757 (to A. S. L.), and NS35439 (to T. Z. B. and Y. N.). This work was also supported by the Brain Research Foundation (to D. M. C.) and the Dutch Epilepsy Fund (NEF #08-01; to W. J. W. and Y. N.).

[S] The on-line version of this article (available at http://www.jbc.org) contains supplemental Figs. 1–3.

[1] Both authors contributed equally to this work.

[2] To whom correspondence should be addressed: 303 E. Chicago Ave., Ward Bldg Room 10-201, Chicago, IL 60611. Tel.: 312-503-4362; Fax: 312-503-0872; E-mail: d-chetkovich@northwestern.edu.

[3] The abbreviations used are: HCN, hyperpolarization-activated cyclic nucleotide-gated; CNBD, cyclic nucleotide binding domain; TRIP8b, tetratricopeptide repeat-containing Rab8b-interacting protein; CNG, cyclic nucleotide-gated; PEX5, peroxin 5; pF, picofarads; TPR, tetratricopeptide repeat; ANOVA, analysis of variance.

unknown. Because interactions between PEX5 and cargo C-terminal tripeptides are important for translocating PEX5 cargo from the cytoplasm to the peroxisomal matrix, we suspected that the interaction between the TRIP8b TPR domains and the HCN subunit C-terminal tripeptides could be important for the trafficking effects of distinct TRIP8b isoforms. The effects of TRIP8b on HCN channel gating and kinetics are the opposite of the effects of cAMP, and indeed TRIP8b reversibly blocks cAMP effects on HCN2 channel function (9). Whereas we found direct interaction between TRIP8b and the HCN1 C-linker and CNBD, it has remained unknown if TRIP8b and cAMP compete for the same site on the CNBD. In this study we address the distinctive roles of the two interaction sites of TRIP8b and HCN channels using biochemical, cell biological, and electrophysiological approaches.

EXPERIMENTAL PROCEDURES

Cloning—All restriction enzymes were purchased from New England Biolabs. All oligonucleotides for use in PCR amplification and oligo insertion were synthesized by Integrated DNA Technologies (Coralville, IA). The proper introduction of all mutations and deletions was verified by DNA sequencing.

Nomenclature of Constructs and Mutations—To simplify naming of TRIP8b constructs, we now prefer the naming system used by Santoro *et al.* (11) for TRIP8b alternatively spliced isoforms. Thus, TRIP8b_IsoA2 described in Lewis *et al.* (10) is TRIP8b(1a-2-4) (11), wherein 1a-2-4 indicates inclusion of alternatively spliced exons 1a, 2, and 4. Furthermore, because different N-terminal splice isoforms all have different residue numbering in the conserved TPR domains, we introduced a naming scheme that identifies mutations based on the sequential number of the TRIP8b TPR domain (1–6) and the amino acid residue number (1–34) within that specific TPR domain. Thus, a mutation of Asn-13 of TPR domain 3 to Ala in any TRIP8b isoform is indicated with the designation "TPR3-N13A." In TRIP8b(1a-2-4), for example, this mutation is represented as TRIP8b(1a-2-4)[TPR3-N13A].

cDNA Plasmids—The yeast two-hybrid and mammalian expression constructs of HCN1, HCN1-HA, and wild type TRIP8b were described previously (10). Point mutations in TRIP8b were introduced in pGAD-TRIP8b(1c). First, using two-part PCR to generate overlapping fragments, a silent XbaI site was introduced in exons encoding TPR2-C27 and -L28, and then a silent AgeI site was introduced in exons encoding TPR5-R16 and -S17. TPR domain mutations were introduced into this new TRIP8b(1c) clone containing silent XbaI and AgeI sites by PCR mutagenesis using primers and restriction enzyme sites listed in Table 1. pXEC-TRIP8b(1a-2-4)[TPR3-N13A] was made by inserting the EcoRV/BamHI fragment from pGAD-TRIP8b(1c)[TPR3-N13A] into pXEC-TRIP8b(1a-2-4) at the same sites. A construct containing the Δ58 mutation was made by generating a PCR fragment encoding residues 20–220 of TRIP8b(1a-2-4) and inserting this at the NcoI/EcoR I sites of fragment pGAD-TRIP8b(1c) to make pGAD-TRIP8b(1a-2-4)[Δ58]. pXEC-TRIP8b(1a-2-4)[Δ58] and pXEC-TRIP8b(1a-2-4)[Δ58+TPR3-N13A] were made by inserting the BglII/EcoRV fragment from pGAD-TRIP8b(1a-2-4)[Δ58] into pXEC-

TABLE 1
TRIP8b constructs

cDNA	External 5′	Internal 3′	Internal 5′	External 3′	Cloning sites
TRIP8b(1c)[silentXbaI]	CGC GAA TTC ACC ACC ATG CAG GCA GAA TGG GAG G	GTT GTT GGG CTG CAA CTC TAG ACA CCT CTG GAG GGC G	CGC CCT CCA GAG GTG TCT AGA GTT GCA GCC CAA CAA C	CGC CGC CTC GAG CCC GGG TCA AGG ATC CAA ATT GAA AG	EcoR1/Xho1
TRIP8b(1c)[silentXbaI+AgeI]	CGC CCT CCA GAG GTG TC TAG AGT TGC AGC CCA ACA AC	CCT CCA CAG CTT CCT CAG ACC GGT CTC CAT TTG CCA AG	CTT GGC AAA TGG AGA CCG GTC TGA GGA AGC TGT GGA GG	CGC CGC CTC GAG CCC GGG TCA AGG ATC CAA ATT GAA AG	Xba1/Xho1
TRIP8b(1c)[TPR2-N14A]	CGC GAA TTC ACC ACC ATG CAG GCA GAA TGG GAG G	Not applicable	Not applicable	AAC TCT AGA CAC CTC TGG AGG GCG ACA ATA GCT GCC TGC TCA TTT TCA GCC TCA GCC TGG GTT ATA C	EcoR1/Xba1
TRIP8b(1c)[TPR2-E15K]	CGC GAA TTC ACC ACC ATG CAG GCA GAA TGG GAG G	Not applicable	Not applicable	AAC TCT AGA CAC CTC TGG AGG GCG ACA ATA GCT GCC TGC TCA TTT TTA TTC TCA GCC TGG GTT ATA C	EcoR1/Xba1
TRIP8b(1c)[TPR3-N13A]	CGC GAA TTC ACC ACC ATG CAG GCA GAA TGG GAG G	CCT GCT GGT GGC TGG TGG CGG TGT AAC TTA CAG CC	GGC TGT AAG TTA CAC CGC CAC CAG CCA CCA GCA GG	CGC CGC CTC GAG CCC GGG TCA AGG ATC CAA ATT GAA AG	Xba1/Age1
TRIP8b(1c)[TPR5-N5A]	CGC GAA TTC ACC ACC ATG CAG GCA GAA TGG GAG G	Not applicable	Not applicable	CAG ACC GGT CTC CAT TTG CCA AGG TTG CCC CAA GAC GGG CCC ACA GTG AGT AAT CC	EcoR1/Age1
TRIP8b(1c)[TPR6-R2A]	CGC GAA TTC ACC ACC ATG CAG GCA GAA TGG GAG G	CAG GTT GTA TCT GGA GGC GAT GAA ACC TGG CTG G	CCA GCC AGG TTT CAT CGC CTC CAG ATA CAA CCT G	CGC CGC CTC GAG CCC GGG TCA AGG ATC CAA ATT GAA AG	Age1/Xho1

TABLE 2
CNBD constructs

cDNA	5′ Primer	3′ Primer	Cloning sites
pGBK-T7-HCN1-(453–591)	CGC GAA TTC TTC AAC TGC CGG AAA CTG G	CGG GGA TCC TCA CAG GAG AAT AGA GTT	EcoRI/BamHI
pGBK-T7-HCN2-(439–644)	CGC GAA TTC ATC CAG TCC CTG GAT TCG TC	CGC GGA TCC GTC GAC TCA CAG CAA GAT GGA GTT CTT CTT G	EcoRI/BamHI
pGBK-T7-HCN3-(349–554)	CGC AAG CTT GTC GAC CTA TCC AGT CCC TGG ACT CTT CC	CGC GGT ACC GCG GCC GCT CAC TGC AGT ATC GAA TTC TTT TTG CCG	SalI/NotI
pGBK-T7-HCN4-(517–722)	CGC GAA TTC ATC CAG TCC CTG GAC TCC TCC CGG	CGC AAG CTT GTC GAC TCA GAG GAG GAT GGA GTT CTT CTT GCC	EcoR I/SalI
pGBK-T7-CNGA2-(380–583)	CTC CAC CAT GGA TGC CAC ACG AGC AG	ATA TAT GGA TCC TCA TTC CTT CAT CAG GAT CTC	NcoI/BamH1
pGBK-T7-CNGA3-(471–612)	CGC GAA TTC AAC GTG CAC CTG GAC ACG	CGC GGA TCC CGG GTC AGA TCA GGT TGT CTT TCA TC	EcoRI/BamHI
pGBK-T7-CNGA4-(272–475)	CGC GCG CCA TGG ACA CTG CAG ATG CGG CCT TC	ATA TAT GGA TCC TCA CAT TTT AAG CAA GAT TTC	NcoI/BamH1
pGBK-T7-CNGB3-(513–652)	CAT ATG GCC ATG GAC GAT GTG AAC TTC AGC ATC	CGC GGA TCC CGG GTC AGG TCT TAG CCT TCT GC	NcoI/BamH1

TRIP8b(1a-2-4) or pXEC-TRIP8b(1a-2-4)[TPR3-N13A], respectively.

For CNBD yeast two-hybrid constructs, template plasmids encoding mouse HCN1 and HCN2 were provided by Steven Siegelbaum. Template plasmids encoding mouse HCN3 and human HCN4 were provided by Martin Biel (Universität München). Template plasmids encoding rat CNG2, CNGA4, sea urchin SpIH, and mouse KCNH1 (ether-a-go-go) were provided by William Zagotta (University of Washington). Plasmids encoding human CNGA3 and CNGB3 were provided by K.-W. Yau (Johns Hopkins) and Michael Varnum (Washington State University), respectively. cDNA fragments SpIH(470–655) and KCNH1(505–702) were cut from parent plasmid pMAL-C2T with HindIII (blunted with Klenow), and NcoI was then inserted into yeast two-hybrid bait vector pGBK-T7 at NcoI/SmaI. Other CNBD clones were obtained by PCR of the parent plasmids to amplify cDNA encoding the CNBD plus 17 N-terminal and 4 C-terminal amino acids followed by subcloning into yeast two-hybrid bait vector pGBK-T7. Table 2 lists the primers and restriction sites used.

TRIP8b Protein Expression Constructs—cDNA encoding TRIP8b(1a) and TRIP8b(1c) were cloned into pETM30 at Nco1/Xho1.

Yeast Two-hybrid Assays—Directed yeast two-hybrid interaction assays were performed as previously described (13).

Co-Immunoprecipitation Assays—Co-immunoprecipitation of HCN and TRIP8b from transfected human embryonic kidney 293 (HEK293T) cells (ATCC) and surface HA-tagged HCN1 immunoprecipitation were performed as described previously (10).

Preparation of Purified GST Fusion Proteins—Fusion protein was expressed in BL21 bacteria (Stratagene) and purified by glutathione-Sepharose affinity chromatography (Amersham Biosciences) according to manufacturer's instructions. Protein was quantified by Coomassie Plus Protein Assay Reagent (Thermo), separated into aliquot, and stored at −20 °C.

GST Pulldown Assays—HEK293 cells were transfected with cDNA plasmids encoding HCN1, HCN1[Δ3], HCN1[R538E], or HCN1[Δ3+R538E] and lysed in TEEN-Tx (TEEN buffer (50 mM Tris-HCl, pH 7.4, 1 mM EDTA, 1 mM EGTA and 150 mM NaCl) containing 1% Triton X-100) as described above. After removal of an input fraction, 5 mg of GST-tagged TRIP8b fusion protein was added along with glutathione-Sepharose beads, and the reaction was gently rocked for 2 h at 4 °C. Supernatant was then removed, and beads were washed six times with cold TEEN-Tx followed by the addition of 4× sample buffer and boiling to elute bound proteins. For some experiments, 8-bromoadenosine 3′:5′-cyclic monophosphate or adenosine 3′:5′-cyclic monophosphate (Sigma) was added to the pulldown reaction mixture. IC_{50} was calculated using GraphPad Prism software.

Western Blotting—Western blotting was performed as previously described (14). Primary antibody concentrations used were gp anti-HCN1 (1:3000) and gp anti-TRIP8b (1:3000), and the concentrations of secondary horseradish peroxidase-conjugated rabbit anti-gp antibody were 1:10,000. Densitometric quantization of band intensity was performed using Photoshop. Statistical analyses were performed by ANOVA using GraphPad Prism software, and the significance of intergroup differences was determined using 1-way ANOVA with Tukey's post hoc test. Differences at the level of $p \leq 0.05$ were considered statistically significant.

Flow Cytometry—The surface expression evaluation by flow cytometry was performed as described previously (9). HEK293 cells were transfected with HA-HCN1 and TRIP8b(1a-2-4) wild type and mutations with cell transfected with pEGFP as a control. For the cAMP studies, cells were incubated with 100 μM forskolin (Sigma) for 1 h after 72 h of transfection. Nonpermeabilized cells were stained with mouse anti-HA primary antibody to label surface HA and then were stained with secondary antibody conjugated to Alexa-647 (Invitrogen). Cells were run in a Cyan ADP flow cytometer (Dakocytomation) at the Northwestern University Flow Cytometry Core facility, and data were analyzed by FloJo software. The presented fluorescence index was calculated as the integral of the Alexa-647 fluorescence with respect to cell number, which was normalized by eGFP-positive cells in each transfection condition. The fluorescence indices for each condition were normalized to the control transfection condition (HCN1 plus eGFP). Statistical analyses were performed using 1-way ANOVA with Tukey's post hoc-test.

Electrophysiological Measurements in HEK293 Cells—HEK293 cells for electrophysiological measurements were grown and maintained as previously described (15). 1–2 days

before transfection, cells were trypsinized and re-plated on 12-mm glass coverslips at 50–60% density. Transfection with plasmid cDNA was performed 2–3 days after plating using the calcium-phosphate precipitation method. A vector encoding the wild type mouse HCN1 channel was co-transfected with various TRIP8b constructs at a 1:1 ratio (0.6 μg of DNA per construct per coverslip) alongside a vector encoding eGFP (0.06 μg/coverslip) to visualize transfected cells.

Whole-cell patch clamp recording was performed 24–48 h post-transfection. A coverslip containing transfected HEK293 cells was placed in a bath chamber of an inverted Olympus IX-70 microscope and was continuously perfused with an extracellular solution containing 110 mM NaCl, 5 mM KCl, 2 mM $CaCl_2$, 1 mM $MgCl_2$, and mM 10 HEPES (pH set to 7.30). Recording pipettes were pulled from borosilicate glass and had a resistance of 2–4 megaohms when filled with an intracellular solution containing 105 mM potassium gluconate, 30 mM KCl, 2 mM Mg-ATP, 5 mM EGTA, 0.5 mM $CaCl_2$, and 10 mM HEPES (pH set to 7.30). Series resistance was <15 megaohms and was compensated for at least 70%. Under these conditions, voltage errors originating from uncompensated series resistance were in almost all cases lower than 1 mV and never higher than 2 mV.

Whole-cell voltage clamp was realized with an Axopatch 200B amplifier (Molecular Devices) controlled by a custom-made program written in MATLAB (Mathworks). Currents were low-pass Bessel filtered at 2 kHz. The currents were sampled at 5 kHz by a custom-made program written in MATLAB that also controlled the amplifier and generated the voltage commands. Voltages were offline corrected for liquid junction potentials (calculated as 13 mV).

I_h was evoked by a series of hyperpolarizing steps from a holding potential of −40 to −130 mV in decrements of −10 mV. Analysis of electrophysiological data was performed using custom-written procedures in MATLAB. The amplitude of I_h was quantified as the difference between the current measured immediately after the beginning of the hyperpolarizing step and the steady state current determined at the end of the pulse. Current density was calculated using the cell capacitance as read from the compensation dial on the amplifier. The cell capacitance (quantified at 14.4 ± 0.4 picofarads, $n = 111$ cells) did not differ across the various experimental conditions (one-way ANOVA).

Activation kinetics were best fit to a single exponential function, and all current traces included in the final analysis had a goodness-of-fit value above 0.98. We investigated whether adding a second or third exponential to the fit would lead to a considerable improvement of the fit, but this was hardly ever the case in our preparation. As would have complicated statistical comparison, we did not include these results in the further analysis.

The voltage-dependent current as measured above results from the voltage-dependent activation and the driving force as best described by the Goldman-Hodgkin-Katz equation,

$$I(V) = g(V) \times V \times \frac{[\mathrm{Ion}^+]_{in} - \exp(\alpha V)}{[\mathrm{Ion}^+]_{out} \quad 1 - \exp(\alpha V)} \qquad \text{(Eq. 1)}$$

with $\alpha = F/RT$, where $g(V)$ is the voltage-dependent conductance of I_h, F the Faraday constant, R the gas constant, and T represents the absolute temperature; for Ion_{in} and Ion_{out} we used concentrations that yielded the correct Nernst equilibrium potential for I_h ($E_{rev} = -36$ mV). The voltage dependence of $g(V)$ was well described by a Boltzmann equation,

$$g(V) = \frac{g_{max}}{1 + \exp\left(\frac{v - v_{SD}}{v_s}\right)} \qquad \text{(Eq. 2)}$$

where g_{max} is the maximal conductance, V is the holding potential, V_{50} is the voltage of half-maximal activation, and V_s is a slope factor (in mV).

All data points are given as the means ± S.E. Statistical comparison between groups was performed using an ANOVA followed by a Dunnett post-hoc test or by the non-parametric Kruskal-Wallis ANOVA with multiple testing using Dunn-Sidak correction. Statistical analysis was performed using SPSS software (Version 18.0, SPSS Inc.) and MATLAB. $p < 0.05$ was considered to indicate a significant difference.

RESULTS

Two Distinct Interaction Domains of TRIP8b and HCN1—In previous work, we demonstrated that TRIP8b interactions with HCN1 occur at distinct sites in both TRIP8b and HCN1 (10). Binding to the C-terminal tripeptide of HCN1 (SNL) required the C-terminal portion of TRIP8b, including both sets of TPR domains. Additionally, we found a second interaction site with HCN1 that required a 58-amino acid segment in the N terminus upstream of the TPR sets. This second binding domain interacted with an HCN1 construct containing only the intracellular C-linker and cyclic nucleotide binding domain (HCN1-(386–591); HCN1-CNBD+). We performed a further deletion of 4–6 of the C-linker helices (HCN1-(453–591); HCN1-CNBD) and found that an intact CNBD, but not C-linker, is required for this interaction (Fig. 1*A*). For clarity, we refer to these two interactions hereafter in this manuscript as NC (for TRIP8b N terminus, HCN CNBD) and TT (for TRIP8b TPR domains, HCN Tripeptide).

To evaluate the structural architecture of these distinct interaction sites, we performed mutagenesis to disrupt NC or TT interactions in a full-length TRIP8b isoform known to dramatically up-regulate HCN1, TRIP8b(1a-2-4). As a preliminary screen we utilized directed yeast two-hybrid screens to characterize effects of mutations in disrupting either NC or TT interactions. We found that wild type TRIP8b(1a-2-4) interacted with HCN1 C-terminal fragments containing the C-terminal tripeptide (with no CNBD) or the CNBD (with no tripeptide) (Fig. 1*A*). Wild type TRIP8b(1a-2-4) also interacted with fragments containing either the C-terminal tripeptide or the CNBD from HCN2, HCN3, and HCN4, indicating both the NC and TT interactions occur with all HCN isoforms. We next made a full-length TRIP8b(1a-2-4) construct containing a deletion of the 58 amino acid residues upstream of the TPR domains required for the HCN1 NC interaction, TRIP8b(1a-2-4)[Δ58]. TRIP8b(1a-2-4)[Δ58] did not interact with any HCN CNBD but did interact with all HCN subunit constructs containing the

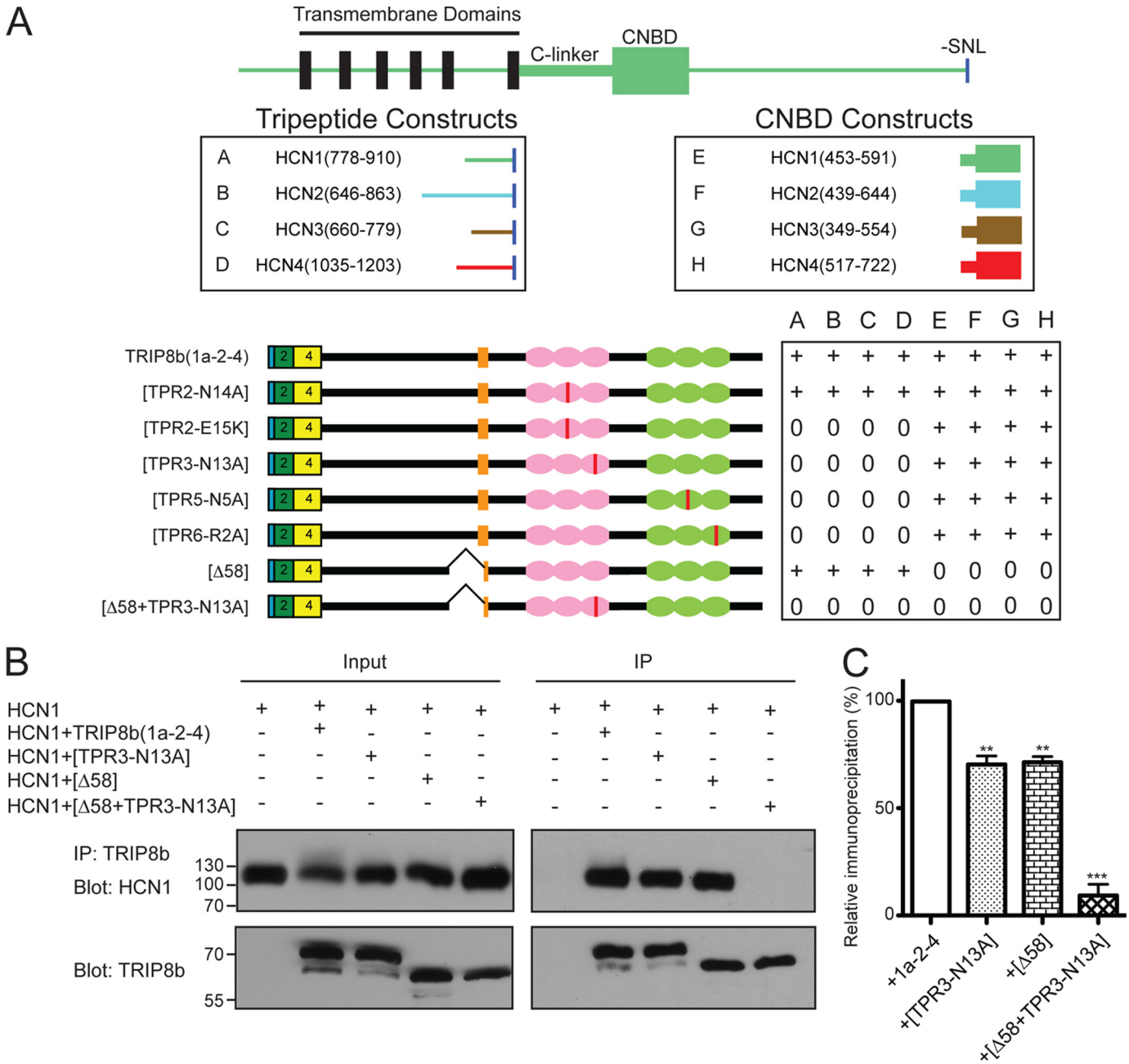

FIGURE 1. **TRIP8b interacts with HCN channels at two distinct sites**. *A*, schematic representations of HCN subunit and TRIP8b constructs tested in directed yeast two-hybrid interactions are shown. The + indicates auxotrophic growth resulting from interaction of bait and prey plasmids, whereas 0 signifies no interaction. *B*, Western blots of extracts from HEK293T cells transfected with HCN1 and the indicated TRIP8b constructs were immunoprecipitated with α-TRIP8b and probed with α-HCN1 (*top panels*) or α-TRIP8b (*bottom panels*). Input is 6% that of the total lysate, whereas immunoprecipitate (*IP*) is 15%. Molecular mass markers are shown in kDa. *C*, shown are summary data for interaction of HCN1 and TRIP8b. ** and ***, $p < 0.01$ and 0.001, respectively, *versus* TRIP8b(1a2–4), 1-way ANOVA with Tukey's post hoc test, $n = 3$).

C-terminal tripeptide (Fig. 1*A*). Thus, the mutation of TRIP8b(1a-2-4)[Δ58] selectively eliminates interaction with the HCN(1–4) CNBD.

We next sought to create mutations in TRIP8b to disrupt the TT interaction with the HCN subunit C-terminal tripeptide. We took advantage of the homology of TRIP8b and PEX5 combined with the knowledge of PEX5 structure (12) and extensive information about functional mutagenesis (16, 17) to design TRIP8b constructs predicted to disrupt binding to the terminal three amino acids (SNL). By aligning TRIP8b and PEX5 sequences, residues that are important for PEX5 binding to SKL were identified in TRIP8b (supplemental Fig. 1). We then created PEX5 homologous mutations in full-length TRIP8b. Using yeast two-hybrid assays, we identified four point mutations in four distinct TRIP8b TPR domains that disrupted TT interaction (TPR2-E15K, TPR3-N13A, TPR5-N5K, and TPR6-R2A), none of which affected binding to HCN constructs containing the CNBD (Fig. 1*A*). The PEX5 C-loop at the C terminus after the TPR domains is important for some PEX5 cargo binding (12), and we similarly found that deletion of the TRIP8b residues C-terminal to the sixth TPR domain also disrupted HCN tripeptide binding (data not shown). We next generated a

TABLE 3

Biophysical properties of I_h in the presence of various TRIP8b(1a-2-4) mutants

Biophysical properties of I_h in HEK293 cells co-transfected with HCN1 and various TRIP8b(1a-2-4) mutants are shown. Differences in current density were assessed using Kruskal-Wallis test ($p < 0.001$) followed by post hoc Mann-Whitney tests with a Dunn-Sidak correction. Other comparisons were made using ANOVA ($p < 0.001$ for τ; $p < 0.01$ for both V_{50} and k) with a post hoc Dunnett test. All data points are the mean ± S.E.

Construct	I_h density	τ at −110 mV	V_{50}	Slope factor/k
	pA/pF	*ms*		*mV*
HCN1	7.4 ± 1.7	132 ± 14	−80.1 ± 0.8	5.2 ± 0.3
	(n = 24)	(n = 6)	(n = 7)	(n = 7)
HCN1 +TRIP8b(1-a2-4)	33.8 ± 5.4[a]	182 ± 8 [b]	−84.0 ± 0.8[c]	5.2 ± 0.2
	(n = 23)	(n = 14)	(n = 15)	(n = 15)
HCN1+	19.4 ± 4.3	200 ± 10[b]	−86.6 ± 1.4[b]	5.8 ± 0.2
TRIP8b(1a-2–4)[TPR3-N13A]	(n = 25)	(n = 8)	(n = 7)	(n = 7)
HCN1 +	24.1 ± 4.3[b]	144 ± 8	−80.1 ± 0.8	6.2 ± 0.2
TRIP8b(1a-2–4)[Δ58]	(n = 18)	(n = 9)	(n = 10)	(n = 10)
HCN1 +	9.2 ± 0.9	144 ± 11	−80.2 ± 1.0	6.4 ± 0.4[c]
TRIP8b(1a-2–4)[Δ58+TPR3-N13A]	(n = 22)	(n = 8)	(n = 6)	(n = 6)

[a] $p < 0.001$.
[b] $p < 0.01$.
[c] $p < 0.05$.

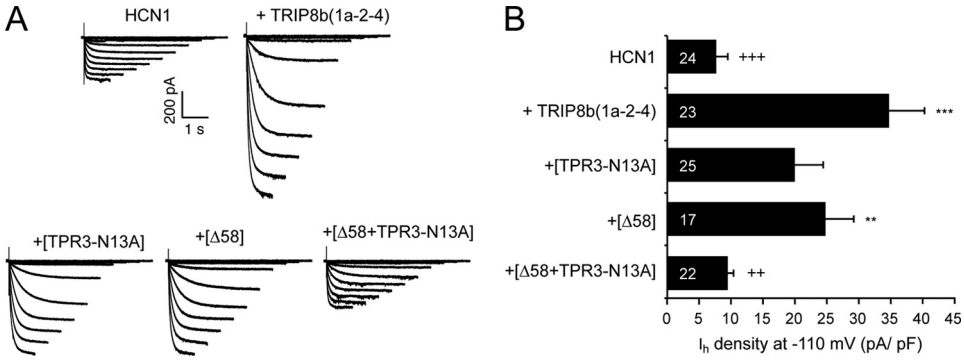

FIGURE 2. **TRIP8b interaction with the HCN1 CNBD and the C-terminal tripeptide contribute to TRIP8b-mediated increases in HCN1 current density.** *A*, example I_h traces recorded from transfected HEK293 cells in response to a series of hyperpolarizing steps (from −40 to −130 mV in decrements of −10 mV) are shown. Cells were transfected with HCN1 alone (*left trace*) or co-transfected with both HCN1 and TRIP8b(1a-2-4) mutants as indicated. *B*, shown is a quantitative summary of I_h density in HEK293 cells co-transfected with HCN1 and TRIP8b(1a-2-4) mutants. ** and ***, $p < 0.01$ and 0.001, respectively, compared with the current density of HCN1 when expressed alone. ++ and +++, $p < 0.01$ and 0.001, respectively, compared with currents obtained upon transfection of HCN1 with wild type TRIP8b(1a-2-4). No. of cells is indicated per experimental group on the *bar histogram*.

TRIP8b construct with mutations predicted to completely disrupt interactions with HCN subunits. As shown in Fig. 1*A*, the double mutant construct TRIP8b(1a-2-4)[Δ58+TPR3-N13A] was unable to interact with CNBD- or tripeptide-containing HCN constructs in yeast two hybrid assays. The interaction between TRIP8b mutations and HCN1 was next verified by coimmunoprecipitation in HEK293T cells. Consistent with yeast two-hybrid data, wild type TRIP8b(1a-2-4) coimmunoprecipitated robustly with HCN1. Furthermore, both TRIP8b(1a-2-4)[Δ58] and TRIP8b(1a-2-4)[TPR3-N13A] immunoprecipitated HCN1. As predicted, coimmunoprecipitation was abolished in the TRIP8b construct harboring both mutations, TRIP8b(1a-2-4)[Δ58+TPR3-N13A] (Fig. 1, *B* and C).

Interaction with Both the CNBD and the C-terminal Tripeptide of HCN1 Contribute to TRIP8b Regulation of I_h Density—Acting as an auxiliary subunit of the HCN channel complex, TRIP8b interaction influences channel current density and gating (9–11). Utilizing our TRIP8b constructs harboring specific defects in HCN subunit binding, we sought to determine which binding sites between TRIP8b and HCN subunits contributed to this function. We first evaluated TRIP8b effects on current density. Expression of HCN1 alone in HEK293 cells resulted in a mean current density of 7.4 ± 1.7 pA/pF (measured at −110 mV, n = 24, Table 3, Fig. 2). Co-expression of HCN1 with wild type TRIP8b(1a-2-4), a TRIP8b isoform that dramatically up-regulates HCN current (10), markedly enhanced current density (33.8 ± 5.4 pA/pF, $p < 0.001$, Table 3, Fig. 2). Transfection of TRIP8b(1a-2-4) harboring the Δ58 mutation also significantly up-regulated current density as compared with HCN1 alone (24 ± 4.3 pA/pF, n = 17; Table 3, Fig. 2), but values were lower than those obtained with full-length TRIP8b(1a-2-4). Interestingly, expression of HCN1 with the TRIP8b(1a-2-4)[TPR3-N13A] mutant resulted in an intermediate current density with values comparable with those obtained with the TRIP8b(1a-2-4)[Δ58] mutant (19.4 ± 4.3; n = 25; Table 3; Fig. 2). Co-transfection of the double mutant TRIP8b(1a-2-4)[Δ58+TPR3-N13A], which cannot interact with either the CNBD or the C-terminal tripeptide domain of HCN1, generated an HCN1 current density that was comparable with that found with HCN1 alone (9.2 ± 0.9 pA/pF, n = 22, $p > 0.05$, Table 3, Fig. 2). These results suggest that interaction between TRIP8b and both the CNBD and the C-terminal tripeptide SNL contribute to the TRIP8b effect on HCN current.

TRIP8b Interaction with CNBD or C-terminal Tripeptide Regulates Current Density through the Effects on HCN Channel Trafficking—TRIP8b controls current density via regulation of HCN1 surface expression (10, 11). Therefore, we expected that the Δ58 and TPR3-N13A mutants, both enhancing current density, would also enhance surface expression. To measure surface expression, we performed flow cytometry using non-

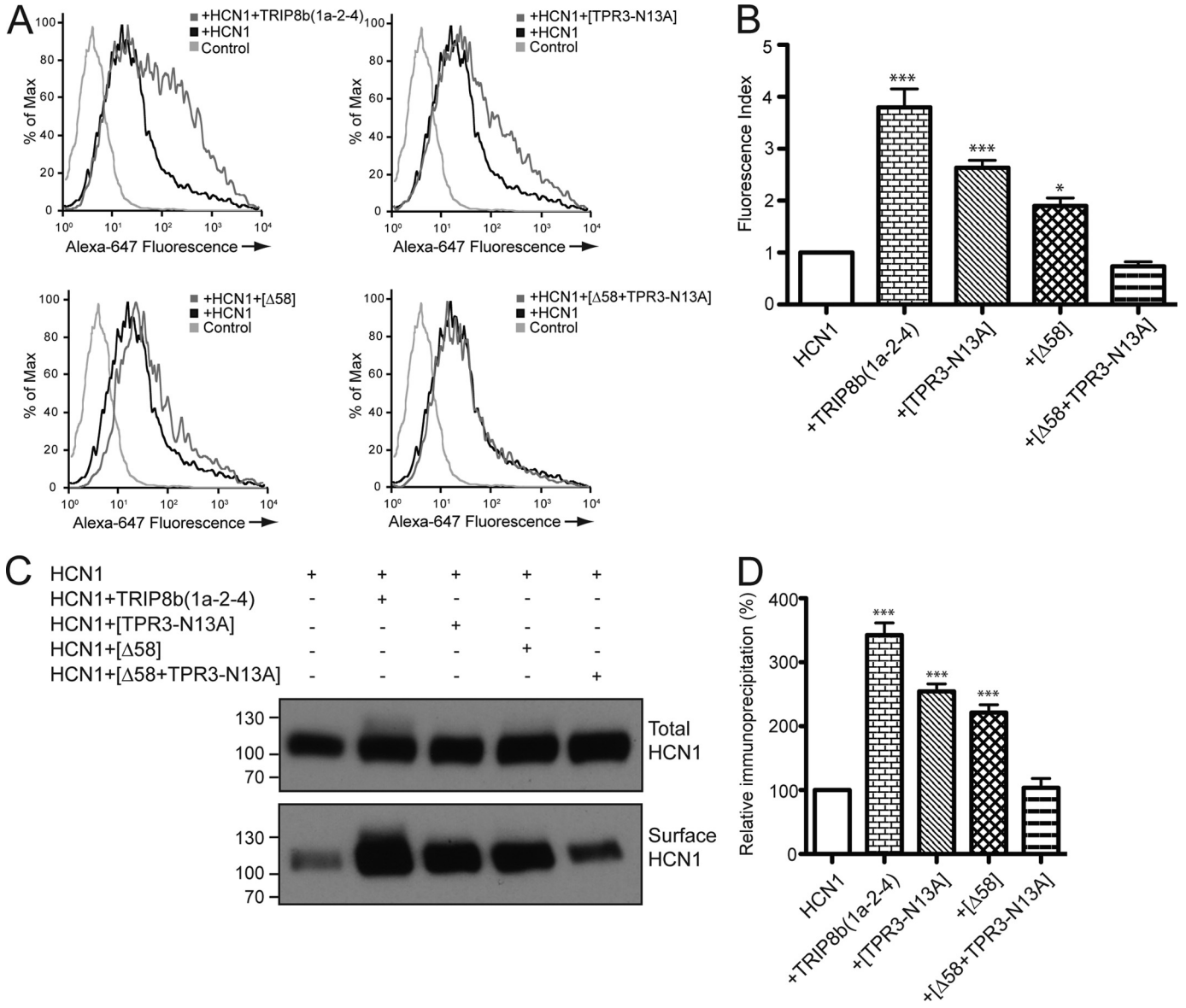

FIGURE 3. **TRIP8b interaction with either the HCN1 CNBD or the C-terminal tripeptide is required for TRIP8b-mediated increases in HCN1 surface expression.** *A*, shown are representative flow cytometric histograms obtained for cells labeled with surface-HA when a construct encoding HCN1-HA was co-expressed with eGFP alone or with eGFP and the indicated TRIP8b(1a-2-4) constructs. The *x* axis indicates the fluorescence intensity in arbitrary units (note the log scale), and the *y* axis indicates the percentage of the maximum cell count. Representative distributions obtained from eGFP-transfected cells (control) were overlaid with each experimental condition as indicated. *B*, summary data for flow cytometric studies of surface expression of HCN1-HA are shown. Compared with HCN1 alone, TRIP8b(1a-2-4), TRIP8b(1a-2-4)[TPR3-N13A], and TRIP8b(1a-2-4)[Δ58] significantly increased the HCN1 surface expression, whereas TRIP8b(1a-2-4)[Δ58+TPR3-N13A] had no effect (***, $p < 0.001$; *, $p < 0.05$, $n = 6$). *C*, representative Western blots of extracts from HEK293T cells transfected with HCN1 and the indicated TRIP8b constructs. Surface HA epitope was bound in non-permeabilized cells before solubilization and immunoprecipitation with α-HA. *D*, summary data for surface HCN1-HA immunoprecipitation are shown. Compared with HCN1 alone, wild type TRIP8b(1a-2-4), TRIP8b(1a-2-4)[TPR3-N13A], and TRIP8b(1a-2-4)[Δ58] significantly increased the amount of HCN1 surface expression, whereas TRIP8b(1a-2-4)[Δ58+TPR3-N13A] had no effect (***, $p < 0.001$, 1-way ANOVA with Tukey's post hoc-test, $n = 3$). Input was 6% of total lysate, and immunoprecipitation was 15%. Molecular mass markers are shown in kDa.

permeabilized HEK293T cells cotransfected with eGFP and different combinations of TRIP8b mutant constructs and HCN1. As shown in Fig. 3, *A* and *B*, wild type TRIP8b greatly increased the surface expression of HCN1 ($p < 0.001$). Both TRIP8b(1a-2-4)[Δ58] and TRIP8b(1a-2-4)[TPR3-N13A] significantly upregulated the HCN1 surface expression TRIP8b(1a-2-4)[TPR3-N13A] *versus* HCN1 $p < 0.001$; TRIP8b(1a-2-4)[Δ58] *versus* HCN1 $p < 0.05$), albeit less than wild type TRIP8b. By contrast, in cells co-transfected with mutant TRIP8b lacking both NC and TT binding sites, HCN1 surface expression levels were similar to transfection with HCN1 alone. These flow cytometry results were confirmed using co-immunoprecipitation of a HA-tagged HCN1 in non-permeabilized HEK293T cells co-transfected with different TRIP8b constructs. Consistent with flow cytometry results, the wild type and singly mutated TRIP8b [TRIP8b(1a-2-4)[Δ58] or TRIP8b(1a-2-4)[TPR3-N13A]) significantly increased the surface expression of HCN1 as compared with control HCN1 alone ($p < 0.001$), whereas TRIP8b 1a-2-4 harboring both mutations did not (Fig. 3, *C* and *D*).

Interaction with the CNBD Domain Is Required for TRIP8b-induced Inhibition of HCN Channel Opening—Previous studies have demonstrated an inhibitory effect of TRIP8b on HCN

channel gating that is manifested in slower activation time constants (τ) and a hyperpolarizing shift of the voltage-activation curve (assessed as the voltage of half-maximal activation, V_{50}) (9–11). Because the CNBD domain is known to play an important role in the regulation of HCN channel gating (5, 6) and because TRIP8b antagonizes effects of cAMP on HCN2 channel function (9), we tested if direct and specific interactions with the CNBD domain mediate the effects of TRIP8b on HCN channel voltage dependence and kinetics.

Confirming previous results (10, 11), co-transfection of HEK293 cells with HCN1 and wild type TRIP8b(1a-2-4) resulted in significantly slowed I_h activation kinetics (Fig. 4) accompanied by a hyperpolarizing shift of the activation curve (Fig. 5, see also Table 3). The Δ58 mutation, which eliminates TRIP8b binding to the CNBD domain, abolished the inhibitory effect of TRIP8b on I_h gating as both the activation kinetics and the voltage-activation were comparable with I_h in cells that were transfected with HCN1 alone (Figs. 4 and 5). In contrast, co-transfection of HCN1 with TRIP8b(1a-2-4)[TPR3-N13A] exerted an inhibitory effect on both I_h kinetics and voltage-dependent activation, similar to the effect of wild type TRIP8b(1a-2-4). Finally, co-transfection of HCN1 with the double mutant TRIP8b(1a-2-4)[(Δ58+TPR3-N13A] yielded similar kinetics and voltage-activation properties to those obtained when HCN1 was expressed either alone or along with the Δ58 mutant. Taken together, these results indicate that whereas current density can be up-regulated by interaction of TRIP8b with either of the two interaction sites on the HCN channel, the effects on channel activation and kinetics are mediated solely by interactions with the CNBD domain.

cAMP Inhibits TRIP8b Interaction with the HCN CNBD—The direct interaction of TRIP8b with the HCN1 CNBD to affect channel activation is consistent with prior findings suggesting that TRIP8b is a competitive antagonist of the functional effects of cAMP on HCN2 activation (9). To determine whether cAMP directly antagonizes the interaction between TRIP8b and the HCN CNBD, we performed GST pulldown assays in the presence of cAMP concentrations from 0 to 1 mM, a range that includes concentrations below and above saturation of cAMP effects on I_h voltage gating (18) (Fig. 6, *A* and *B*). Graded concentrations of cAMP did not significantly impair the interaction of TRIP8b with an HCN1 construct containing an intact C-terminal tripeptide. However, increasing amounts of cAMP reduced the binding of TRIP8b to an HCN1 construct lacking the C-terminal tripeptide in a concentration-dependent manner, with an IC_{50} of 40 nM ($n = 3$). This inhibition of TRIP8b binding to the HCN1 CNBD by cAMP indicates that TRIP8b and cAMP might compete at overlapping binding sites to regulate HCN channel gating.

The crystal structure of mouse HCN2 has demonstrated that cAMP interacts directly with the highly conserved Arg-591 (Arg-538 in HCN1) within the CNBD, leading to allosteric changes coupled to gating (5, 19, 20). Mutation of HCN1 Arg-538 (or HCN2 Arg-591) to glutamate (HCN1[R538E]) eliminates the effects of cAMP on channel function without altering the ability of channels to be regulated by voltage (5). If TRIP8b and cAMP compete for binding to the same site in the CNBD, we reasoned that R538E mutation might prevent TRIP8b binding. We performed a directed yeast-two hybrid assay between TRIP8b(1a-2-4) and an HCN1 CNBD construct harboring the R538E mutation (HCN1-(386–591)[R538E]) and found the R538E mutation indeed blocked binding of TRIP8b to the CNBD (Table 4).

To confirm this finding, we also performed GST pulldown assays. We purified a full-length TRIP8b construct that included the CNBD binding domain (GST-TRIP8b(1a)) as well as a construct lacking the 58 amino acids required for CNBD binding (GST-TRIP8b(1c)). We then performed Western blotting after GST pulldown from extracts prepared from HEK cells transfected with wild type HCN1, HCN1[R538E], HCN1[Δ3], and double mutant HCN1[Δ3+R538E] (Fig. 6*C*). In agreement with yeast two-hybrid results, immunoblotting for HCN1 demonstrated markedly decreased binding between TRIP8b(1a) and HCN1[Δ3+R538E]. We also performed a similar GST pulldown of cells transfected with HCN2, HCN2[R591E], HCN2[Δ3], and double mutant HCN1[Δ3+R591E] and also observed markedly decreased binding between TRIP8b(1a) and HCN1[Δ3+R591E] (supplemental Fig. 2). Taken together, these data indicate that HCN1 Arg-538 (Arg-591 in HCN2) was required for the binding of both TRIP8b and cAMP, suggesting that their binding sites at the HCN CNBD overlap.

Because the overall structure of the CNBD, including the importance of a critical Arg for cAMP binding, is shared by other cyclic nucleotide-binding proteins (supplemental Fig. 3 and Flynn *et al.* (21)), we wondered if TRIP8b might bind to other cyclic nucleotide-gated channels. In directed yeast two-hybrid studies, although TRIP8b interacted with the CNBD of all HCN subunits (Fig. 1*A*), it did not interact with the CNBD of olfactory or retinal cyclic nucleotide gated channels CNGA1–4, CNGB1, or CNGB3, nor did it bind the CNBD of the ether-a-go-go-like K^+ channel subunit, KCNH1 (Table 4). TRIP8b also failed to interact with the CNBD of the sea urchin HCN channel, SpIH. These results suggest that the presence of the critical Arg is required but not sufficient to define an overlapping binding site of TRIP8b and cAMP in the CNBD of cyclic-nucleotide regulated K^+ channels. This implies that TRIP8b-mediated inhibition of cAMP effects may not be a general phenomenon in this group but may rather be specific for vertebrate HCN channels.

cAMP Regulates TRIP8b-mediated Effects on HCN1 Trafficking—Previous studies demonstrated that increasing cAMP levels reverses TRIP8b inhibition of HCN2 gating and kinetics (9). Because we found that TRIP8b interaction with the HCN CNBD affected both channel activation and trafficking, we tested if dissociation of the TRIP8b/HCN1 interaction by cAMP might impair the effects of TRIP8b on surface expression of the HCN1 subunit. We performed flow cytometry studies in untreated HEK293 cells and HEK293 cells treated with forskolin to increase intracellular cAMP levels, evaluating surface HCN1 expression in cells transfected alone or together with TRIP8b constructs. As shown in Fig. 6*D*, forskolin treatment had little effect on HCN1 surface expression when the channel was expressed alone (30% reduction, $n = 6$) or when coex-

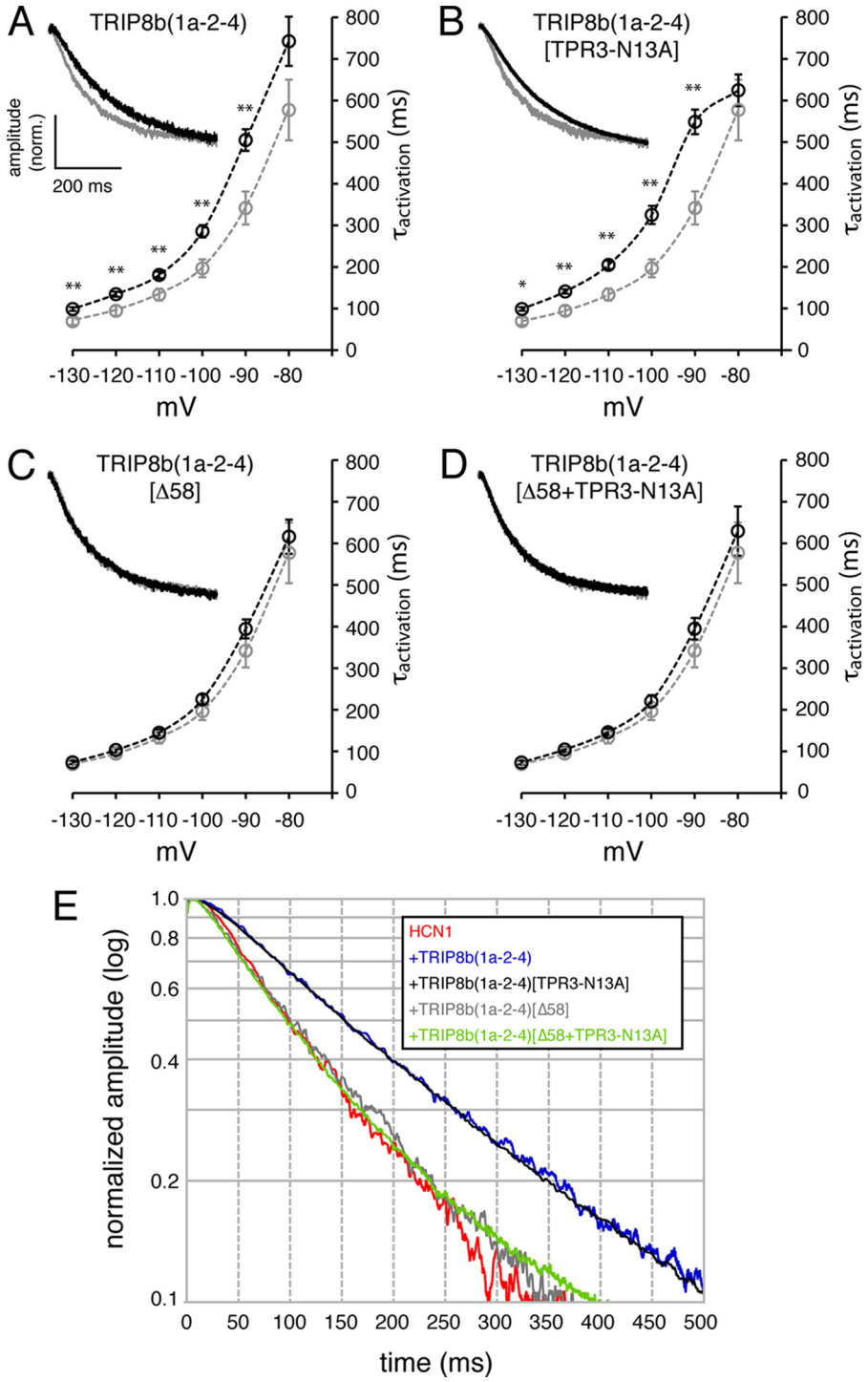

FIGURE 4. **Slowing of HCN1 activation kinetics by TRIP8b is mediated exclusively by interaction with the CNBD interaction domain.** *A–D*, I_h activation kinetics in HEK293 cells expressing HCN1 and various mutants of TRIP8b(1a-2-4) are shown. *Gray data points* represent the activation kinetics of HCN1 when transfected without TRIP8b (the same in all *four panels*), and *black data points* represent the activation kinetics when HCN1 was co-transfected with various TRIP8b(1a-2-4) mutants, as indicated. *Insets* are example traces comparing I_h (evoked by a hyperpolarizing step to −110 mV) in the presence (*black*) and absence (*gray*) of the indicated TRIP8b mutant. Only the first 500 ms of the response are shown. *E*, comparison of all traces is shown in the *insets* to *panel A-D*. The currents were normalized to the amplitude at the end of the pulse (3 s) and are presented at logarithmic scale for demonstration purposes. Statistical comparison of time constants at specific voltages to their counterparts in control cells was performed using ANOVA followed by Dunnett's post hoc test; $n = 6–15$ cells per data point. * = $p < 0.05$; ** = $p < 0.01$.

pressed with wild type TRIP8b(1a-2-4) (20% reduction, $n = 6$). However, when coexpressed with a TRIP8b molecule that increases HCN1 surface expression only via interaction with the CNBD, TRIP8b(1a-2-4)[TPR3-N13A], forskolin reduced HCN1 surface expression by 80% ($n = 6$, $p < 0.001$ *versus* HCN1). These results are intriguing because they indicate that cAMP and TRIP8b directly compete for a CNBD site that governs channel surface expression.

DISCUSSION

The principal findings of these studies are 1) TRIP8b functions as an auxiliary subunit of HCN channels by interacting

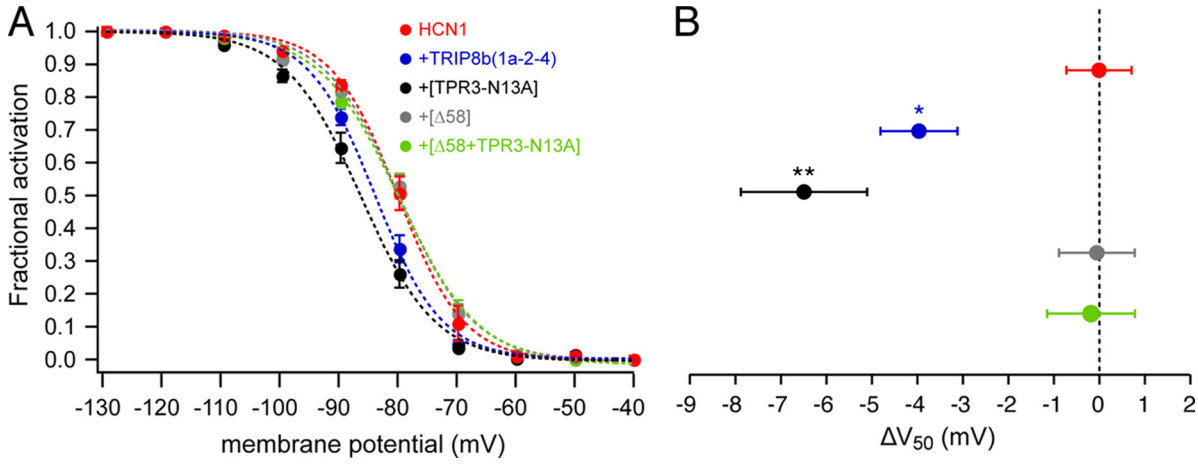

FIGURE 5. **The hyperpolarizing shift in the voltage activation of HCN1 channels by TRIP8b is mediated solely by interaction of HCN1 with the CNBD interaction domain.** *A*, activation curves are based on I_h recorded in HEK293 cells expressing HCN1 together with different TRIP8b mutants as indicated. Deletion of the CNBD-interacting domain (Δ58) resulted in a voltage activation curve not different from the one obtained when HCN1 is transfected alone, whereas interference with the C′-terminal -tripeptide interacting domain (*TPR3-N13A*) resulted in a hyperpolarizing shift of the activation curve similar to that obtained with wild type TRIP8b(1a-2-4). For illustration purposes, the curves presented in this figure are based on grouped and normalized data, whereas statistical analysis of V_{50} and the slope factor was performed on the parameters obtained from the individual Boltzmann fits. *B*, shown is quantification of the effects of mutations on the shift in half-maximal activation V_{50}. See Table 3 for values and statistical significance.

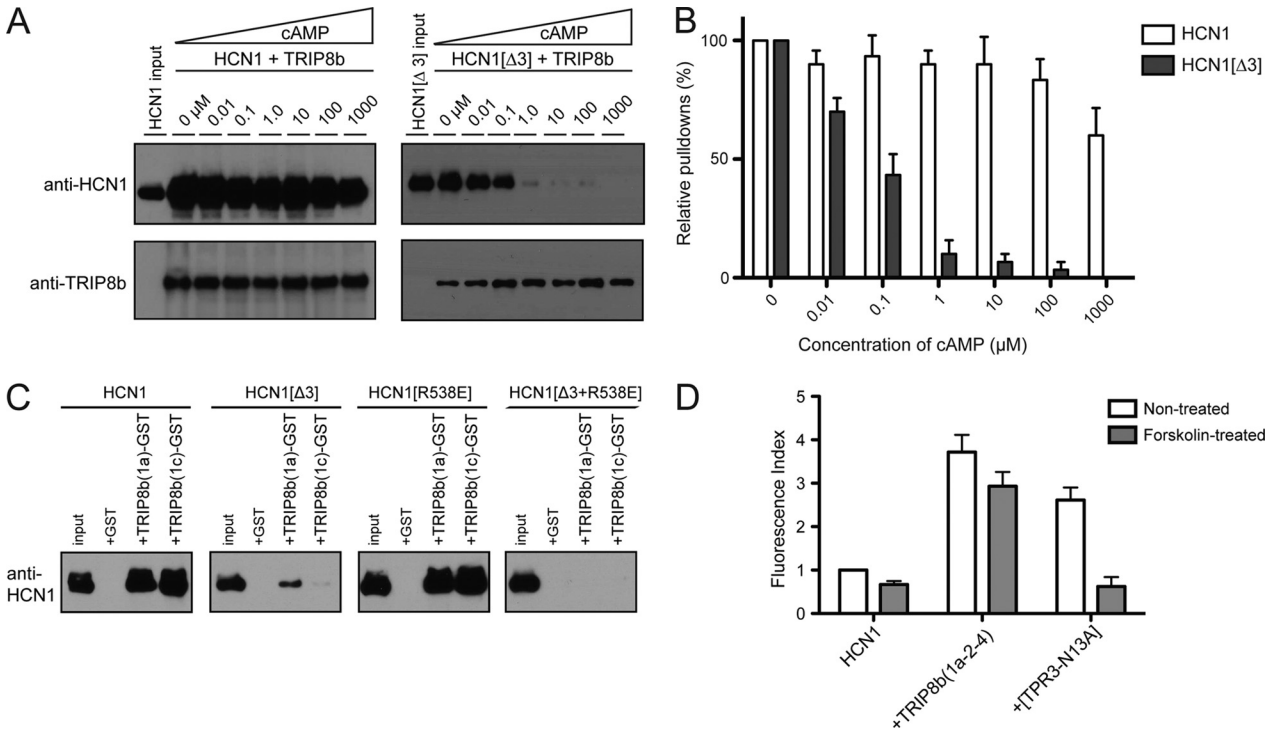

FIGURE 6. **cAMP disrupts TRIP8b-CNBD interactions and their functional effects.** *A* and *B*, Western blots from GST pulldown experiments are shown. *Input* is 15% of lysate precipitated. *A*, extracts from HEK293T cells transfected with HCN1 (*left panels*) or HCN1Δ3 (*right panels*) were incubated with purified recombinant TRIP8b(1a)-GST alone or with the indicated concentration of cAMP, then precipitated with immobilized glutathione and probed for HCN1 (*top panels*) or TRIP8b (*bottom panels*). *B*, shown are summary data for cAMP disrupting TRIP8b-CNBD interaction. Values reflect density of bands corresponding to HCN1 constructs precipitated by TRIP8b(1a)-GST, normalized to conditions lacking cAMP. *C*, extracts from HEK293T cells transfected with HCN1, HCN1[Δ3], HCN1[R538E], or HCN1[Δ3+R538E] were incubated with purified recombinant GST alone, TRIP8b(1a)-GST, or TRIP8b(1c)-GST, then precipitated with immobilized glutathione and probed for HCN1. *D*, shown are summary data for flow cytometric studies of surface expression of HCN1-HA obtained for cells labeled with surface-HA. Cells were transfected with a construct encoding HCN1-HA and eGFP alone or with eGFP and the indicated TRIP8b(1a-2-4) constructs. Before flow cytometry, cells were incubated with or without forskolin as indicated.

with HCN1–4 subunits in a complex manner that involves at least two distinct domains to modulate selectively gating and surface expression, 2) whereas HCN surface expression is governed by TRIP8b binding to both the HCN CNBD and the C-terminal tripeptide binding domains, modulation of gating is dependent on the interaction with the CNBD site alone, and 3) direct binding of TRIP8b and cAMP to the HCN CNBD domain leads to competitive modulation of HCN channel surface expression.

The original identification of TRIP8b as an HCN channel-interacting partner identified the TPR/tripeptide interaction site and also revealed the importance of this interaction for

TABLE 4
CNBD yeast two-hybrid interactions

Prey vector	Interaction with TRIP8b(1a-2-4)
pGBK-T7-HCN1-(386–591)	++
pGBK-T7-HCN1-(386–591)[R538E]	0
pGBK-T7-CNGA2-(380–583)	0
pGBK-T7-CNGA3-(471–612)	0
pGBK-T7-CNGA4-(272–475)	0
pGBK-T7-CNGB3-(513–652)	0
pGBK-T7-KCNH1-(505–702)	0
pGBK-T7-SpIH-(470–655)	0

mediating the trafficking effects of a TRIP8b isoform, TRIP8b(1b-2), that resulted in a down-regulation of HCN channel function (22). Here we find that a TRIP8b isoform that enhances HCN function, TRIP8b(1a-2-4), also employs the TPR/tripeptide interaction in regulating channel trafficking. Importantly, the current study identifies a second binding site involving the TRIP8b residues N-terminal to the TPR domains and the HCN CNBD that is also important for TRIP8b-mediated regulation of HCN1 trafficking. Thus, only when both interactions were eliminated did we block TRIP8b-mediated up-regulation of HCN surface expression.

In addition to contributing to TRIP8b-mediated effects on channel trafficking, we find that this second interaction site alone regulates TRIP8b effects on HCN1 gating. Prior studies demonstrated that TRIP8b acts as a competitive antagonist of cAMP function on HCN2 gating (9). We show here that the mechanism for TRIP8b antagonism of cAMP effects is via direct binding to the CNBD. We found that the interaction between TRIP8b and the CNBD was competitively blocked by increasing concentrations of cAMP and that the concentration at which cAMP inhibited 50% of TRIP8b binding to the HCN1 CNBD (40 nM) was similar to that reported for shifting the $t_{1/2}$ of I_h mediated by HCN1 in oocytes (60 nM) (5). These data are consistent with the possibility that TRIP8b binds to and stabilizes the non-cAMP bound CNBD conformation, whereas conformational changes induced by cAMP (19) eliminate TRIP8b binding. Alternatively, TRIP8b and cAMP might share overlapping binding sites. Along these lines, mutation of a conserved Arg residue in the HCN1 or HCN2 CNBD demonstrated that this residue was necessary for both cAMP and TRIP8b binding. Crystallization of the CNBD in the presence of TRIP8b should help resolve the structural mechanisms by which cAMP and TRIP8b compete at the CNBD.

Although we found TRIP8b interacted with the CNBDs of HCN1-HCN4, it is important to note that TRIP8b did not bind the CNBD of CNG channel subunits, suggesting that TRIP8b is not a general antagonist of cAMP effects on CNBD-containing proteins. It is also notable that TRIP8b did not bind the CNBD of the sea urchin HCN subunit, SpIH. SpIH and other invertebrate HCN channel proteins (*i.e.* fruit fly, spiny lobster, honeybee, Egyptian mosquito) show tremendous diversity in their C termini and all lack the tripeptide SNL conserved across most vertebrate HCN channels. These observations suggest that an important role for TRIP8b in HCN channel function evolved more recently and is consistent with the gene encoding TRIP8b (*Pex5l*) being present only in chordates. Nonetheless, further studies will be required to determine whether TRIP8b is specific for antagonizing cAMP effects only on vertebrate HCN channels.

Intriguingly, we find that the interaction between TRIP8b and the HCN1 CNBD contributed to the trafficking effects of TRIP8b on the HCN channel. Also surprising was the observation that forskolin was able to regulate the trafficking effects of TRIP8b in a TRIP8b construct that interacted only with the HCN CNBD domain. It remains unclear whether cAMP might play a role in regulating trafficking of HCN channels in the brain, where neuronal activity that typically augments cellular cAMP levels promotes HCN1 membrane expression (23). TRlP8b may facilitate HCN channel internalization via interactions with adapter proteins such as AP-2 (11), and it is interesting to speculate that cAMP in neurons might contribute to dissociation of TRlP8b from HCN channels and increase their surface expression. Future experiments are planned to evaluate further the role cAMP might play in regulating TRlP8b-mediated trafficking effects *in vivo*.

In summary, the results of our study give insight into the functional importance of two distinct interactions between HCN1–4 subunits and TRIP8b. Whereas both interactions contribute to TRIP8b regulation of current density and intracellular trafficking, unique interaction with the HCN CNBD allows TRIP8b to regulate gating. Our data further suggest that regulation of HCN channel function by TRIP8b is closely linked to cAMP metabolism, as cAMP antagonizes the effects of TRIP8b on HCN function by directly disrupting the interaction between TRIP8b and the HCN CNBD.

Acknowledgments—We thank Quratul-Ain Ismail and Andrey B. Popov for technical support.

REFERENCES

1. Robinson, R. B., and Siegelbaum, S. A. (2003) *Annu. Rev. Physiol.* **65,** 453–480
2. Santoro, B., and Baram, T. Z. (2003) *Trends Neurosci.* **26,** 550–554
3. Biel, M., Wahl-Schott, C., Michalakis, S., and Zong, X. (2009) *Physiol. Rev.* **89,** 847–885
4. Lewis, A. S., and Chetkovich, D. M. (2011) *Mol. Cell. Neurosci.* **46,** 357–367
5. Chen, S., Wang, J., and Siegelbaum, S. A. (2001) *J. Gen. Physiol.* **117,** 491–504
6. Wainger, B. J., DeGennaro, M., Santoro, B., Siegelbaum, S. A., and Tibbs, G. R. (2001) *Nature* **411,** 805–810
7. Wang, J., Chen, S., and Siegelbaum, S. A. (2001) *J. Gen. Physiol.* **118,** 237–250
8. Lewis, A. S., Estep, C. M., and Chetkovich, D. M. (2010) *Channels* (*Austin*) **4,** 215–231
9. Zolles, G., Wenzel, D., Bildl, W., Schulte, U., Hofmann, A., Müller, C. S., Thumfart, J. O., Vlachos, A., Deller, T., Pfeifer, A., Fleischmann, B. K., Roeper, J., Fakler, B., and Klöcker, N. (2009) *Neuron* **62,** 814–825
10. Lewis, A. S., Schwartz, E., Chan, C. S., Noam, Y., Shin, M., Wadman, W. J., Surmeier, D. J., Baram, T. Z., Macdonald, R. L., and Chetkovich, D. M. (2009) *J. Neurosci.* **29,** 6250–6265
11. Santoro, B., Piskorowski, R. A., Pian, P., Hu, L., Liu, H., and Siegelbaum, S. A. (2009) *Neuron* **62,** 802–813
12. Stanley, W. A., and Wilmanns, M. (2006) *Biochim. Biophys. Acta* **1763,** 1592–1598
13. Cuadra, A. E., Kuo, S. H., Kawasaki, Y., Bredt, D. S., and Chetkovich, D. M. (2004) *J. Neurosci.* **24,** 7491–7502

14. Shin, M., Brager, D., Jaramillo, T. C., Johnston, D., and Chetkovich, D. M. (2008) *Neurobiol. Dis.* **32,** 26–36
15. Noam, Y., Wadman, W. J., and van Hooft, J. A. (2008) *J. Physiol.* **586,** 3629–3638
16. Klein, A. T., Barnett, P., Bottger, G., Konings, D., Tabak, H. F., and Distel, B. (2001) *J. Biol. Chem.* **276,** 15034–15041
17. Shimozawa, N., Zhang, Z., Suzuki, Y., Imamura, A., Tsukamoto, T., Osumi, T., Fujiki, Y., Orii, T., Barth, P. G., Wanders, R. J., and Kondo, N. (1999) *Biochem. Biophys. Res. Commun.* **262,** 504–508
18. Pian, P., Bucchi, A., Decostanzo, A., Robinson, R. B., and Siegelbaum, S. A. (2007) *Pflugers Arch.* **455,** 125–145
19. Zagotta, W. N., Olivier, N. B., Black, K. D., Young, E. C., Olson, R., and Gouaux, E. (2003) *Nature* **425,** 200–205
20. Zhou, L., and Siegelbaum, S. A. (2007) *Structure* **15,** 655–670
21. Flynn, G. E., Black, K. D., Islas, L. D., Sankaran, B., and Zagotta, W. N. (2007) *Structure* **15,** 671–682
22. Santoro, B., Wainger, B. J., and Siegelbaum, S. A. (2004) *J. Neurosci.* **24,** 10750–10762
23. Noam, Y., Zha, Q., Phan, L., Wu, R. L., Chetkovich, D. M., Wadman, W. J., and Baram, T. Z. (2010) *J. Biol. Chem.* **285,** 14724–14726